Distinguishing Elastic Shear Deformation from Friction on the Surfaces of Molecular Crystals

Vivek Kalihari,[1] Greg Haugstad,[2] and C. Daniel Frisbie[1]

[1]*Department of Chemical Engineering and Materials Science, University of Minnesota, Minneapolis 55455, USA*

[2]*Characterization Facility, University of Minnesota, Minneapolis 55455, USA*

(Received 26 October 2009; published 26 February 2010)

Elastic deformation on the surfaces of molecular crystals can be imaged using a variant of lateral force microscopy in which the tip is scanned parallel to the cantilever axis. The shear force transverse to this direction has a distinctly different origin than the friction force as determined by the tip velocity and temperature dependence of the cantilever torque. An elastic deformation model for the tip-sample interaction predicts the crystallographic anisotropy of the transverse shear contrast, establishing its connection with the relative magnitude of the in-plane elastic tensor components.

DOI: 10.1103/PhysRevLett.104.086102 PACS numbers: 68.37.Ps, 46.55.+d, 61.66.Hq, 62.20.D−

Over the past two decades conventional lateral force microscopy (LFM), also known as friction force microscopy (FFM), has become the primary tribological technique for examining the atomic and molecular basis of friction at surfaces because it detects frictional forces on a nanometer length scale, allowing precise correlation with structure [1–4]. On the surfaces of molecular materials such as Langmuir-Blodgett films and polymers, FFM has been employed to relate sliding friction to molecular structure and dynamics, for example, low frequency vibrational motions of molecules [5], crystallographic anisotropy [6], and polymer side-group rotations [7,8]. Because of the continuing importance of LFM as a primary tribological method, understanding the origin of shear forces at the tip-sample interface remains an important area of investigation.

In this work, we demonstrate that an unconventional mode of LFM can distinguish between sliding friction and elastic shear deformation at the surfaces of molecular single crystals. Specifically, when the LFM scan vector is perpendicular to the cantilever axis, as in case of FFM, the cantilever twists due to torque on the tip resulting from friction forces at the tip-sample interface. However, aligning the scan vector *parallel* with the cantilever axis while still monitoring cantilever twist, a mode we term the transverse shear microscopy (TSM) [9–12], affords improved sensitivity to elastic shear deformation at the crystal surface. Scanning along particular crystallographic directions in the transverse shear mode generates a cantilever torque that can be related quantitatively to the elastic modulus tensor of the crystal. The velocity and temperature dependencies of both the transverse shear and friction signals confirm that the transverse shear response has a fundamentally different physical origin than friction.

The general usefulness of LFM to sense transverse shear, and thereby to discern the elastic modulus tensor, has been either unrecognized or unexploited. We expect it to be general across broad classes of crystalline, soft materials. The quantitative interpretation of transverse shear contrast that we provide here offers an approach for examining elastic anisotropy and corresponding bonding anisotropy at the surfaces of molecular materials. For many samples, especially thin films, determining elastic anisotropy by TSM may be far simpler than bulk shear modulation or tensile testing methods. In addition, it is likely that an understanding of elastic anisotropy in crystalline organic materials will also impact understanding of the interrelationships between intermolecular bonding and other properties such as optical (refractive index) anisotropy, and thermal or electrical conduction anisotropy.

Our investigations focus on single crystals of a benchmark crystalline organic semiconductor, pentacene ($C_{22}H_{14}$), that has application as the charge transporting layer in organic field effect transistors [13,14]. Figure 1(a) shows an optical image of a pentacene single crystal along with its crystal structure and the unit cell in the **a**-**b** plane. It also demonstrates the herringbone packing of pentacene molecules with a molecular tilt along the $[\bar{1}\,\bar{1}\,0]$ diagonal. Charge carrier mobility is an important figure of merit in semiconductors and a significant anisotropy in field effect mobility has been reported for various organic semiconductors including pentacene [15,16]. This anisotropy reflects anisotropy in intermolecular interactions in organic semiconductors which should also be reflected in the elastic properties.

Single crystals of pentacene were grown from a high purity source (99.8%) through horizontal physical vapor transport and they were indexed using a Bruker diffractometer fitted with an area detector. The TSM and FFM experiments were conducted on a Molecular Imaging PicoPlus SPM (now Agilent model 5500): this is an environmentally controlled, tip-scanned system with a sample heating stage. Humidity was kept constant at ~20% throughout the experiments. The probes used for AFM experiments were uncoated silicon ''diving board'' cantilevers with integrated contact mode tips fabricated by MikroMasch, USA (model NSC36 and force constant ~0.95 Nm^{-1}). Each probe was used for both TSM and

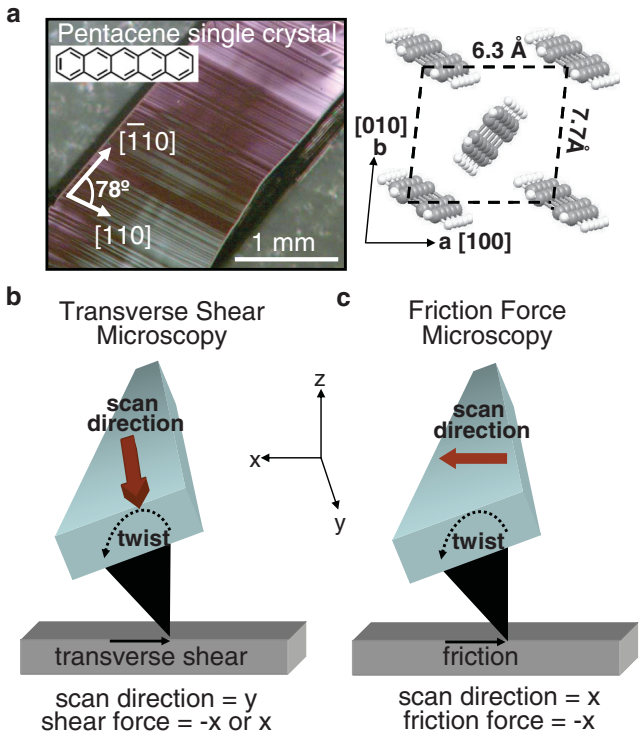

FIG. 1 (color). (a) An optical micrograph of pentacene along with its molecular structure and the unit cell in **a**-**b** plane. It also demonstrates the herringbone packing of pentacene molecules with a molecular tilt along the $[\bar{1}\,\bar{1}\,0]$ diagonal. (b) Schematic showing the working mechanism of the TSM, where the scan direction is parallel to the cantilever axis. (c) Schematic showing the working mechanism of the conventional FFM, where the cantilever axis and the scan direction are orthogonal.

FFM measurements to remove the tip dependence of the measured signal. Pentacene single crystals were manually rotated under the force microscope in order to measure the TSM and FFM signals along different crystallographic directions. A constant normal load (~2 nN) was applied during the variable temperature and velocity experiments. During the variable temperature experiment, the cantilever deflection set point was adjusted after every temperature step using force curve analysis in order to compensate for thermal drift.

In our previous reports [10,11], we demonstrated that the TSM signal depends on the relative orientation between a crystallographic direction and the cantilever scan vector (fast scan direction). Figure 1(b) shows the schematic of TSM, where the scanning direction of a probe tip is parallel to the cantilever and the signal corresponds to the orthogonal twist of the compliant cantilever. The only operational difference between TSM and conventional FFM is the scanning direction, i.e., in FFM the scanning direction is perpendicular to the cantilever axis [Fig. 1(c)]. The alignment of the scan vector along the cantilever axis in TSM means that any twist of the cantilever results from the net shear forces acting in a direction transverse to the scanning direction.

Figure 2(a) shows three examples of frictional loops with positive trace and negative retrace signals, at different crystal temperatures. Similar trace-retrace loops are observed in TSM as well [Fig. 2(b)] and are used to measure the TSM signal. In FFM, the frictional force is proportional to the width of trace-retrace "friction loops." The FFM trace scan always induces a clockwise twist of the cantilever (a positive signal from the photodetector that monitors the cantilever-reflected laser spot displacement) and the retrace scan always induces a counterclockwise twist (negative signal). Therefore, the measured frictional force (proportional to trace minus retrace scan) is always positive. Importantly, the friction loops (trace or retrace) may show spikes due to abrupt changes in topography which cancel out after calculating the difference of the two signals. In TSM, the trace scan can result in either clockwise or counterclock twist and the retrace scan results in the opposite twist. Hence, a TSM signal (proportional to trace minus retrace scan) can be either positive or negative. In Fig. 2(b), the TSM signal (trace minus retrace scan) is positive.

The conventional approach to analyze friction is to study the friction as a function of tip velocity [7,8,17], sample temperature [7,8,18], and applied normal load [19]. In order to understand the fundamental difference between TSM and FFM, we followed the same approach and mea-

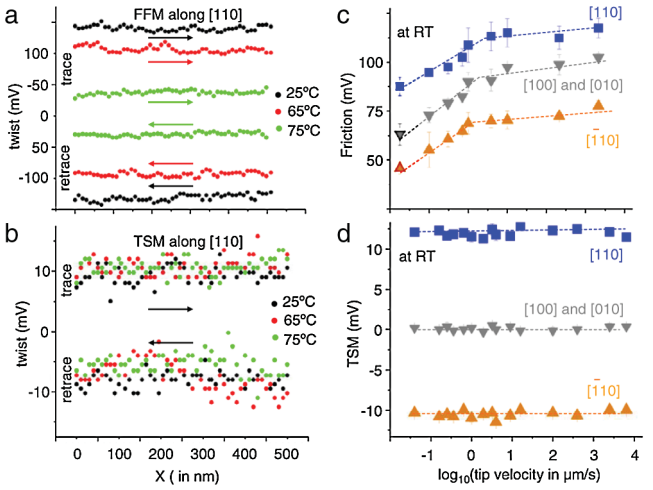

FIG. 2 (color). (a) Friction loops (trace and retrace scans) as a function of pentacene crystal temperature. The width of the friction loops decreases with an increase in temperature. (b) TSM loops as a function of pentacene crystal temperature. The width of the TSM loops remains constant with an increase in temperature. (c) Semilogarithmic plot of friction versus tip-velocity at room temperature along different crystallographic directions on an indexed pentacene crystal. At lower velocity regime (less than 1 μm/s), the friction increases with tip-velocity but saturates at higher velocities (greater than 1 μm/s). (d) Semilogarithmic plot of TSM versus tip-velocity at room temperature. The TSM signal shows anisotropic behavior, but remains constant as a function of tip-velocity over 5 orders of magnitude.

sured the TSM and FFM signals as a function of velocity and sample temperature on an indexed pentacene single crystal.

Figure 2(c) plots the friction as a function of logarithmic velocity along different crystallographic directions at room temperature. The plot clearly indicates that the friction is initially velocity dependent and anisotropic. The magnitude of the friction is highest along the diagonal [110] and lowest along the other diagonal [$\bar{1}$10]. Along the **a** axis [100] and the **b** axis [010] there is no significant difference in friction (both the directions are represented by a single curve) and the friction magnitude lies between those along the two diagonals. There is a logarithmic increase of friction with velocity in the lower velocity regime (0.1–1.0 μm/s) and constant friction in the higher velocity regime (greater than 1.0 μm/s). This trend is observed for all the crystallographic directions as shown in the Fig. 2(c). Similar friction dependence on tip velocity has been experimentally observed and rationalized by a modified Tomlinson model [17,20], where at lower velocities the atomic friction increases logarithmically with velocity due to the thermally activated hopping of the contact atoms, but at higher velocities friction is constant as thermal activation ceases to be relevant.

On the other hand, the TSM response, Fig. 2(d), is completely independent of velocity over 5 orders of magnitude at room temperature. Like friction, TSM is anisotropic, i.e., the TSM signal is positive along [110], *negative* along [$\bar{1}$10], and zero for both the **a** [100] and **b** [010] axis. Importantly, the absence of velocity dependence for the TSM signal indicates that the physical origin of the transverse shear force is fundamentally different from friction.

In order to gain more insight into the difference between the FFM and TSM signals, we measured their dependence on crystal temperature. Figures 2(a) and 2(b) show friction and TSM loops at different crystal temperatures, respectively. It is evident from the plot that the friction loops collapse (the signal gets smaller), whereas the TSM loops remain constant with an increase in crystal temperature. The loops presented in Figs. 2(a) and 2(b) were taken along [110], but the other crystallographic directions also showed similar behavior. This observation is consistent with expectations that friction is thermally activated, while transverse shear is not. Further, we probed the origin of friction by performing the conventional time-temperature superposition analysis and calculated the activation energy for friction (see supplementary material [21]).

The different velocity and temperature dependence of friction and transverse shear clearly indicates that their physical origins are different. Specifically, the absence of velocity and temperature dependence for the TSM signal suggests that it is related to elastic deformation at the tip-sample interface. To probe this hypothesis, we developed a mathematical model using the theory of linear elasticity [22] describing elastic deformation acting at a tip-sample interface. This model is a substantial improvement of our previous model which proved only that the TSM signal will be zero for an isotropic material independent of the scanning direction [10]. The improved model is general and can be used to calculate the elastic deformation and hence, the TSM signal in terms of the components of the elastic tensor for any material (derivation in Supporting Information). The general equation describing the TSM signal in an image plane containing principal directions (1 and 2) is given by

$$\begin{aligned}\mathrm{TSM} = G[&E_{1111}(-\cos^3\theta\sin\theta) + E_{2222}(\cos\theta\sin^3\theta)\\ &+ 2E_{1212}(2\cos^3\theta\sin\theta - 2\cos\theta\sin^3\theta)\\ &+ E_{1122}(\cos^3\theta\sin\theta - \cos\theta\sin^3\theta)\\ &+ 2E_{1112}(-3\cos^2\theta\sin^2\theta + \cos^4\theta)\\ &+ 2E_{2212}(3\cos^2\theta\sin^2\theta - \sin^4\theta)],\end{aligned}$$

where G is a lumped constant with units of V/Pa describing the cantilever-tip geometry, the sample strain, the tip-sample contact area, and the instrument sensitivity, θ is the angle between the scanning direction and the principal direction 1, and E_{ijkl} are components of the fourth order elastic modulus tensor with units of Pa.

The above equation for the TSM signal describes the cantilever twist based on the components of the in-plane elastic modulus tensor and it goes to zero for an isotropic material. To model the TSM data for pentacene, we inserted the reported elastic constants for an anthracene single crystal [23], as the elastic constants for pentacene are unknown. The similar molecular structure and herringbone packing of anthracene and pentacene molecules makes anthracene's elastic constants an excellent choice, as the relative magnitudes of different elastic constants should be similar in the two organic crystals. For the TSM calculations, we took the 1-2 plane as the **a**-**b** plane because the crystal plane under analysis is the **a**[100]-**b**[010] plane of pentacene. Figure 3(a) shows the experimental TSM data (filled triangles) obtained on a pentacene single crystal and the calculated TSM signal (solid line) based on the reported elastic constants of an anthracene single crystal. The good agreement between the mathematical model and the experimental results indicates that the origin of TSM is elastic anisotropy at the sample surface, and that the elasticity model can predict the TSM signal. Thus, fitting the data in Fig. 3(a) could also be used to calculate (or refine in this case) the relative **a**-**b** plane elastic constants for pentacene single crystals which are $E_{1111} \sim 0.6E_{2222}$, $E_{1212} \sim 0.1E_{2222}$, $E_{1122} \sim 0.3E_{2222}$, $E_{1112} \ll E_{2222}$, and $E_{2212} \ll E_{2222}$. Furthermore, in order to emphasize the importance of the relative magnitudes of the tensor components in calculating the TSM signal, we explored the sensitivity of the fit to changes in the elastic constants. The dotted line in Fig. 3(a), for example, represents the modified TSM plot when the value of E_{1212} is increased by ~60% and all the other in-plane elastic constants are kept unchanged. The difference in the original (solid line) and the modified (dotted line) TSM plot clearly

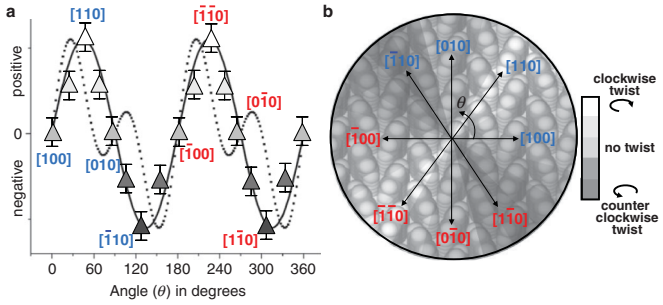

FIG. 3 (color). (a) Plot of TSM signal versus scanning direction (θ). Excellent agreement between the experimental TSM measurements (filled triangles) and the modeled TSM signal (solid line) indicates that the origin of TSM is elastic anisotropy at the sample surface. Thus, fitting the data in the figure could also be used to calculate (or refine in this case) the relative **a**-**b** plane elastic constants for pentacene single crystal which are: $E_{1111} \sim 0.6E_{2222}$, $E_{1212} \sim 0.1E_{2222}$, $E_{1122} \sim 0.3E_{2222}$, $E_{1112} \ll E_{2222}$, and $E_{2212} \ll E_{2222}$. The figure also shows another calculated TSM plot (dotted line) with E_{1212} increased by 60%, demonstrating that even a small change in the relative magnitude of the in-plane elastic tensor components can drastically change the shape of the predicted TSM response. (b) Schematic showing the angular dependence of TSM signal overlaid on a pentacene single crystal structure.

indicates that the calculated TSM signal is sensitive to the relative magnitudes of in-plane elastic tensor components and even a small change can drastically change the shape of the predicted TSM response.

Figure 3(b) is a scheme depicting the angular dependence of the TSM signal (or image contrast) on a pentacene single crystal structure. The color variation in the diagram demonstrates that the TSM signal is zero for scan directions along the **a** [100] and **b** [010] axes. The maximum clockwise (positive) twist is obtained when scanning along the [110] diagonal, whereas maximum counterclockwise (negative) twist is obtained when scanning along the $[\bar{1}10]$ diagonal.

The detection of elastic shear deformation by TSM of course implies that such deformation also occurs in conventional FFM, as expected. However, comparison of the TSM and friction signals in Fig. 2 reveals that the TSM signal is at least a factor of 10 smaller, meaning that in FFM the effects of elastic deformation on sliding friction are masked by the much larger contributions of activated, stick-slip behavior to the total friction signal. The reason TSM is sensitive to elastic deformation is that when the scan vector is parallel to the cantilever, the activated, stick-slip phenomena are much less likely to generate a torque about the cantilever axis.

In conclusion, we have demonstrated that elastic shear deformation forces on molecular surfaces can be cleanly detected using a variant of lateral force microscopy, termed transverse shear microscopy. Tip velocity and temperature-dependent measurements demonstrate that both conventional FFM and TSM reveal anisotropy on crystalline organic surfaces, but that FFM is activated while TSM is nonactivated. A linear elasticity model accurately captures the TSM response in terms of the components of the in-plane elastic modulus tensor of the material, which in turn indicates that the relative magnitude of the in-plane tensor components can be determined from the crystallographic dependence of the TSM contrast. In addition, the ability to image elastic anisotropy at high resolution is useful for microstructural characterization of soft materials, and for relating other physical properties (e.g., optical, thermal or electrical anisotropy) to bonding anisotropy in such systems.

This work was partially supported by the MRSEC Program of the National Science Foundation under Grant No. DMR-0212302 and No. DMR-0819885. Partial support was provided by NSF through DMR-0706011. Parts of this work were carried out in the Institute of Technology Characterization Facility, University of Minnesota, which received partial support from NSF through the NNIN and MRSEC programs.

[1] C. M. Mate *et al.*, Phys. Rev. Lett. **59**, 1942 (1987).
[2] R. M. Overney *et al.*, Phys. Rev. Lett. **72**, 3546 (1994).
[3] R. W. Carpick and M. Salmeron, Chem. Rev. **97**, 1163 (1997).
[4] B. Bhushan, *Introduction to Tribology* (John Wiley & Sons, New York, 2002).
[5] E. Barrena *et al.*, Phys. Rev. Lett. **82**, 2880 (1999).
[6] M. Liley *et al.*, Science **280**, 273 (1998).
[7] J. A. Hammerschmidt, W. L. Gladfelter, and G. Haugstad, Macromolecules **32**, 3360 (1999).
[8] S. Sills and R. M. Overney, Phys. Rev. Lett. **91**, 095501 (2003).
[9] K. Puntambekar *et al.*, Adv. Funct. Mater. **16**, 879 (2006).
[10] V. Kalihari *et al.*, Adv. Mater. **20**, 4033 (2008).
[11] V. Kalihari *et al.*, Adv. Mater. **21**, 3092 (2009).
[12] J. Zhang, J. P. Rabe, and N. Koch, Adv. Mater. **20**, 3254 (2008).
[13] D. J. Gundlach *et al.*, IEEE Electron Device Lett. **18**, 87 (1997).
[14] A. Dodabalapur, L. Torsi, and H. E. Katz, Science **268**, 270 (1995).
[15] V. C. Sundar *et al.*, Science **303**, 1644 (2004).
[16] J. Y. Lee, S. Roth, and Y. W. Park, Appl. Phys. Lett. **88**, 252106 (2006).
[17] E. Riedo *et al.*, Phys. Rev. Lett. **91**, 084502 (2003).
[18] Z. Tshiprut, S. Zelner, and M. Urbakh, Phys. Rev. Lett. **102**, 136102 (2009).
[19] D. B. Knorr, T. O. Gray, and R. M. Overney, J. Chem. Phys. **129**, 074504 (2008).
[20] E. Gnecco *et al.*, Phys. Rev. Lett. **84**, 1172 (2000).
[21] See supplementary material at http://link.aps.org/supplemental/10.1103/PhysRevLett.104.086102.
[22] P. L. Gould, *Introduction to Linear Elasticity* (Springer-Verlag, New York, 1983).
[23] H. B. Huntington, S. G. Gangoli, and J. L. Mills, J. Chem. Phys. **50**, 3844 (1969).